

# Reference potentials for adsorption of helium, argon, methane, and krypton in high-silica zeolites

Orhan Talu <sup>a,\*</sup>, Alan L. Myers <sup>b</sup>

<sup>a</sup> Department of Chemical Engineering, Cleveland State University, Cleveland, OH, 44115, USA

<sup>b</sup> Department of Chemical Engineering, University of Pennsylvania, Philadelphia, PA, 19104, USA

## Abstract

Quantitative agreement with experimental data for adsorption of argon, krypton, and methane in high-silica zeolites is achieved with a molecular model, which (1) assumes pairwise additivity of intermolecular forces; (2) ignores partially concealed silicon atoms and lumps their dispersion energy with the oxygen atoms; (3) neglects energy induced by the weak electric field inside silicalite; (4) uses the Lennard–Jones 12-6 potential for gas–gas and gas–solid interactions. The parameters of the Ar–O gas–solid potential are  $\epsilon/k = 93.0$  K and  $\sigma = 3.335$  Å. The gas–solid potential parameters for krypton and methane were calculated from the Ar–O reference potential using Lorentz–Berthelot mixing rules and the principle of corresponding states. The pore volume of silicalite determined from the He–O potential is  $0.175$  cm<sup>3</sup> g<sup>-1</sup>. The local density of gases adsorbed in the pores varies with the strength of the gas–solid potential; at 306 K and 10 bar, the maximum absolute density of methane is about one half the density of liquid methane at its normal boiling point. © 2001 Elsevier Science B.V. All rights reserved.

**Keywords:** Adsorption; GCMC simulations; Reference potentials; Isotheric heat; Silicalite

## 1. Introduction

Adsorption theory relies heavily upon molecular simulation for the interpretation, understanding, and prediction of adsorption in microporous materials. The input to the molecular simulation is the forcefield: the intermolecular potentials for dispersion, electrostatic, and induction energies of gas–gas and gas–solid interactions. Unfortunately, a handbook of reliable potentials with

tabulated constants does not exist and theory is insufficiently developed to calculate these forcefields from the principles of quantum mechanics. Current methods rely upon approximate intermolecular potentials containing parameters, which are extracted from experimental adsorption data, usually at the limit of zero pressure. These potential parameters can then be used to make predictions for other conditions of temperature or loading or for mixtures of gases under all conditions. The potentials are also useful for studying molecular-scale structural details such as energetically preferred sites and orientations, since this kind of information is difficult to obtain by spectroscopic measurements.

\* Corresponding author. Tel.: +1-216-6872571; fax: +1-216-6879220.

E-mail address: talu@csvax.egr.csuohio.edu (O. Talu).

The first step toward the development of a handbook of potential parameters is to determine a reference potential for the dispersion energy of small spherical molecules (argon, krypton, methane) interacting with high-silica materials such as silicalite.

Simulation of adsorption in micropores of zeolites is based upon the reasonable assumption that adsorption on the external surface of the solid is negligible. The bulk fluid is not included explicitly in grand canonical Monte Carlo (GCMC) simulations; its properties are obtained either from an independent simulation or from an equation of state. The simulation box contains at least enough unit cells to ensure periodicity in the boundary conditions. The independent experimental variables are the temperature ( $T$ ) and pressure ( $P$ ). The input variables to the simulation are the structure of the adsorbent, the temperature, and the chemical potential  $\mu(T, P)$  of the bulk fluid as established by its equation of state. The dependent variables from the simulation are the absolute number of molecules contained in the micropores ( $N^a$ ) and the potential energy ( $\phi$ ) of the gas–gas and gas–solid interactions.  $N^a$  is specific adsorption in molecules per unit mass of adsorbent.

The difference between absolute adsorption from simulation ( $N^a$ ) and excess adsorption from experiment ( $N$ ) is negligible for adsorption of vapors near their boiling points. However, in the case of supercritical gases for which the difference is 10% or more, simulation variables must be converted to excess quantities (Myers et al. [1], Sircar [2,3], Talu and Myers [4]) for comparison with experimental data:

$$N = N^a - V_p \rho_b \quad (1)$$

where  $\rho_b(P, T)$  is the density of the bulk fluid and  $V_p$  is the specific pore volume determined by:

$$V_p = \frac{1}{m_s} \int e^{-\phi(r)/kT} dr \quad (\text{for He}) \quad (2)$$

$\phi$  is the helium–solid potential energy for a single helium molecule,  $dr$  is a differential volume element, and  $m_s$  is the mass of solid adsorbent in the simulation box.  $N$  is specific adsorption and  $V_p$  has units of  $\text{m}^3 \text{kg}^{-1}$ . The pore volume deter-

mined from Eq. (2) mimics the experimental measurement of dead space using helium at room temperature and low pressure (Myers et al. [1]; Tulu and Meyers [4]; Neimark and Ravikovitch [5]). In principle, the temperature in Eq. (2) should be the same temperature (typically about 300 K) used to measure the dead space of the sample cell. However, the integral in Eq. (2) is insensitive to temperature; raising the temperature from 300 to 500 K increases  $V_p$  by less than 1%.

For adsorption experiments performed at sub-atmospheric pressure, the bulk density in Eq. (1) is given by the perfect gas law:

$$\rho_b = \frac{P}{kT} \quad (3)$$

## 2. Adsorption second virial coefficient

Potential parameters of the gas–solid potential energy function are extracted from variables extrapolated to zero pressure, which corresponds physically to the interaction of a single adsorbate molecule with the surface of the adsorbent inside its pores. The adsorption second virial coefficient is:

$$B = kT \lim_{P \rightarrow 0} \left( \frac{dN}{dP} \right) \quad (4)$$

The corresponding limit from simulation is:

$$B^a = kT \lim_{P \rightarrow 0} \left( \frac{dN^a}{dP} \right) \quad (5)$$

and it follows from Eq. (1) and Eqs. (3)–(5) that:

$$B = B^a - V_p \quad (6)$$

The second virial coefficient is calculated from the configuration integral:

$$B = \frac{1}{m_s} \int e^{-\phi(r)/kT} dr - V_p \quad (7)$$

and the isosteric heat of adsorption at zero pressure is:

$$Q_{st} = - \frac{\int \phi(r) e^{-\phi(r)/kT} dr}{\int e^{-\phi(r)/kT} dr - m_s V_p} + kT \quad (8)$$

where  $\phi$  is the gas–solid potential energy for a single adsorbate molecule and the integrations are over a representative mass ( $m_s$ ) of solid adsorbent. Given experimental values of  $B$  and  $Q_{st}$ , Eq. (7) and Eq. (8) can be solved for two unknown parameters in  $\phi$ .

At the limit of zero pressure where  $\rho_b \rightarrow 0$ , Eq. (1) indicates that the difference between excess and absolute variables vanishes. However, the difference in the slopes of the absolute and excess adsorption isotherms remains finite even at the limit of zero pressure due to the pore volume ( $V_p$ ) term in Eq. (6). Moreover, the difference between the absolute and excess isosteric heats is finite at the limit of zero pressure due to the  $V_p$  term in the denominator of Eq. (8).

### 3. Molecular model and GCMC simulations

An approximate but convenient and frequently used potential function for the gas–gas and gas–solid dispersion energy is the Lennard–Jones 12-6 potential:

$$\phi_{ij} = 4\epsilon_{ij} \left[ \left( \frac{\sigma_{ij}}{r} \right)^{12} - \left( \frac{\sigma_{ij}}{r} \right)^6 \right] \quad (9)$$

This potential is for spherical adsorbate molecules such as argon, krypton, and possibly methane interacting with each other (gas–gas interactions) or with the oxygen atoms composing the zeolite (gas–solid interactions). Gas–gas potential parameters are evaluated independently from bulk-gas second virial coefficients. Gas–solid potential parameters ( $\epsilon$  and  $\sigma$ ) can be evaluated from adsorption second virial coefficients using Eq. (7) and Eq. (8).

The molecular model assumes pairwise additivity of gas–gas and gas–solid intermolecular energies from Eq. (9), ignores partially concealed silicon atoms and lumps their dispersion energy with the oxygen atoms, and neglects energy induced by the (small) electric field acting upon the adsorbate molecules. The locations of the oxygen atoms were obtained from crystallographic data (Olson et al. [6]).

The GCMC simulations were run to convergence, as defined by reduction in the standard

deviation in  $\phi$  and  $N^a$  to 1–5%. The number of cycles required for convergence varied from 0.5 to 50 million. The simulation box was 12 units cells of silicalite, which is approximately 40 Å on a side and provides periodic boundary conditions. The cut-off radius for the pretabulated gas–solid energy was 100 Å and the cut-off radius for the gas–gas interactions was set at 20 Å.

### 4. Sensitivity of potential parameters to experimental error

The potential parameters of Eq. (9) must be known before the molecular model can be implemented in a simulation. A worthwhile goal is to create a table of effective potential parameters ( $\epsilon$  and  $\sigma$ ) between simple molecules and various zeolites of practical importance. A longer-term goal is a table of effective potential parameters for non-spherical polar molecules, but here the discussion is limited to small non-polar spherical molecules like argon, krypton, and methane.

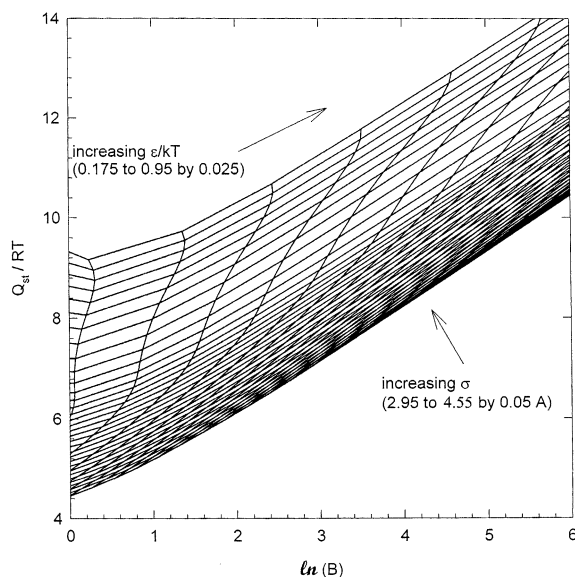


Fig. 1. Lennard–Jones gas–solid potential parameters  $\epsilon$  and  $\sigma$ , which fit experimental values of adsorption second virial coefficient ( $B$  in  $\text{cm}^3 \text{g}^{-1}$ ) and dimensionless isosteric heat ( $Q_{st}/RT$ ) at limit of zero coverage for silicalite ( $V_p = 0.175 \text{ cm}^3 \text{g}^{-1}$ ).

Fig. 1 shows that the extraction of accurate potential parameters from experimental data is surprisingly difficult. Loci for  $2.95 < \sigma < 4.55$  and  $0.175 < (\varepsilon/kT) < 0.950$  are plotted on Fig. 1. In principle, the two constants of the gas–solid interaction potential ( $\varepsilon$  and  $\sigma$ ) can be extracted from experimental values for the adsorption second virial coefficient ( $B$ ) and isosteric heat ( $Q_{st}$ ) at the limit of zero coverage as discussed earlier. For example, for  $\ln(B) = 3$  and  $Q_{st}/kT = 10$ , the solution  $\varepsilon/kT = 0.255$  and  $\sigma = 4.23 \text{ \AA}$  can be read from Fig. 1 at the point  $(x,y) = (3,10)$ . In practice, the values of these parameters are very sensitive to small experimental errors in  $B$  and  $Q_{st}$ . Physical solutions usually are found in the dense lower portion of the families of curves on Fig. 1 where individual loci for constant  $\sigma$  and constant  $\varepsilon$  are difficult to distinguish. Thus there exists a family of solutions for  $\varepsilon$  and  $\sigma$  which reproduce the experimental value of  $B$  and  $Q_{st}$  but have little physical meaning and, therefore, cannot be used for extrapolations to other temperatures or for estimating potential energy functions for other gases and zeolites.

## 5. Determination of argon and helium reference potentials

Both the adsorption second virial coefficient and the isosteric heat at the limit of zero coverage must be converted from absolute to excess quantities using the pore volume ( $V_p$ ) in Eq. (7) and Eq. (8). The pore volume depends on the gas–solid potential for helium, which is unknown at this point. Thus, gas–solid potentials for argon and helium must be extracted simultaneously from the experimental data for argon on silicalite at  $32.6^\circ\text{C}$ :  $B = 4.35 \text{ cm}^3 \text{ g}^{-1}$  and  $Q_{st} = 15.7 \text{ kJ mol}^{-1}$  at the limit of zero pressure (Dunne et al. [7]). Special care was taken to obtain accurate and reproducible experimental values of  $B$  and  $Q_{st}$  for the reasons discussed earlier. Since the potential parameters are more sensitive to the isosteric heat than the second virial coefficient, the probable error in  $Q_{st}$  was reduced to  $0.1 \text{ kJ mol}^{-1}$  by taking a large number (21) of experimental points at low pressure.

Table 1

Lennard–Jones 12-6 potential parameters for adsorption in silicalite

Atom pair	$\varepsilon/k$ (K)	$\sigma$ , ( $\text{\AA}$ )	References
He–He	10.9	2.640	Hirschfelder et al. [8]
Ar–Ar	119.8	3.405	Hirschfelder et al. [8]
O–O	72.2	3.265	This study
He–O	28.0	2.952	Eqs. (10) and (11)
Ar–O	93.0	3.335	Eqs. (10) and (11)

The gas–solid potential constants reported in Table 1 were obtained by a steepest descent optimization routine. The adsorption second virial coefficient and isosteric heat at zero coverage were calculated by integration of  $e^{-\phi/kT}$  and  $\phi e^{-\phi/kT}$  respectively, over the pore volume of silicalite according to Eq. (7) and Eq. (8). The pore volume was calculated from Eq. (2) using the helium–oxygen potential. Values for the helium–oxygen and argon–oxygen potentials were calculated from the customary Lorentz–Berthelot mixing rules:

$$\varepsilon_{ij} = (\varepsilon_{ii}\varepsilon_{jj})^{0.5} \quad (10)$$

$$\sigma_{ij} = \frac{\sigma_{ii} + \sigma_{jj}}{2} \quad (11)$$

The oxygen–oxygen constants in Table 1 ( $\varepsilon$  and  $\sigma$ ) were derived from the optimization routine: the like-pair constants for argon and helium were taken from the literature and the unlike-pair parameters were obtained from Eqs. (10) and (11). The oxygen–oxygen constants, which have no physical meaning beyond their use in Eqs. (10) and (11), were the two unknowns extracted from  $B$  and  $Q_{st}$  using the optimization routine. The pore volume from Eq. (2) obtained by insertion of the optimized helium–oxygen potential constants in Table 1 is  $0.175 \text{ cm}^3 \text{ g}^{-1}$ .

The constants in Table 1 reproduce the experimental adsorption isotherms and isosteric heat measured at room temperature in different laboratories (Dunne et al. [7], Golden and Sircar [9]) for argon in silicalite up to a pressure of about 1000 kPa. Comparison of GCMC simulations with experiment is shown in Fig. 2. The solid line is a best fit of the experiment data. The average

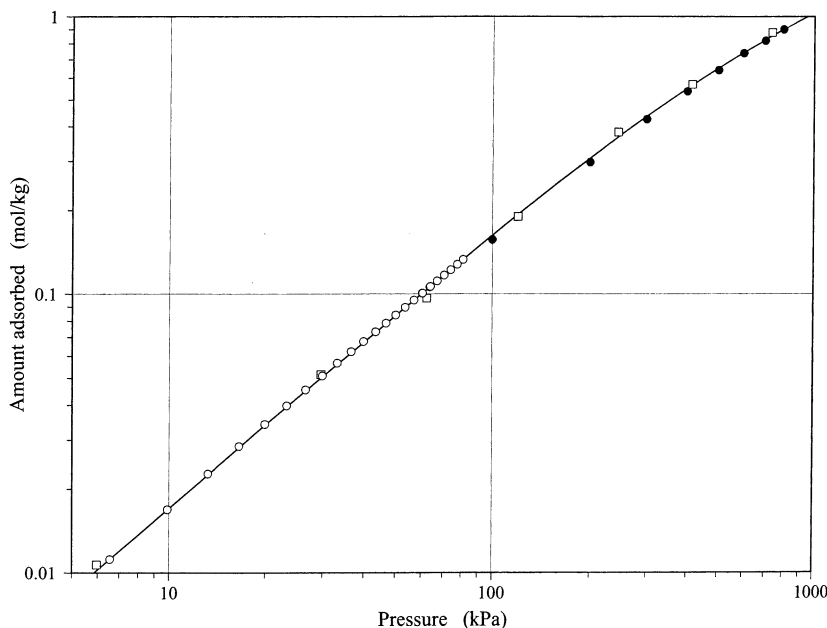


Fig. 2. Comparison of GCMC simulations with experiment for adsorption of argon in silicalite at 32.6°C. ○, experimental data (Dunne et al. [4]); □, experimental data (Golden and Sircar [9]); solid line, best fit of experimental data; ●, GCMC simulation data converted to excess adsorption by Eq. (1).

difference between the GCMC simulations and experiment is less than 2%. The excellent agreement of simulation with experiment implies that the potential parameters have physical significance in spite of their sensitivity to errors in experimental data discussed in the earlier section. The helium–oxygen and argon–oxygen potential parameters in Table 1 are intended to serve as reference values for dispersion interactions of small spherical molecules with oxygen atoms in siliceous materials like silicalite.

Table 2 shows that our Ar–O potential parameters disagree with values obtained by others (Macedonia et al. [10], Smit [11]). The first set (Macedonia et al. [10]) of parameters predicts an isosteric heat which is 3% too low and a Henry constant which is 30% too high. The third set (Smit [11]) predicts an isosteric heat, which is 2% too high and a Henry constant, which is 40% too low. The second set obtained by us agree exactly with the experimental isosteric heat and Henry constant for the argon–silicalite system (Dunne et al. [7]; Golden and Sircar [9]).

## 6. Potential parameters for spherical molecules in siliceous materials

According to the two-parameter principle of corresponding states, the well depth  $\varepsilon$  of the gas–gas potential scales with the critical temperature and the collision diameter scales with the cube root of the critical volume of the adsorbate molecule:

$$\varepsilon \propto T_c \quad (12)$$

$$\sigma \propto V_c^{1/3} \quad (13)$$

Table 3 contains a list of critical constants (Reid et al. [12]) of small molecules which fit into

Table 2  
Sets of Lennard–Jones 12-6 potential parameters for Ar–O in silicate

$\varepsilon/k$ (K)	$\sigma$ , (Å)	References
117.2	3.121	Macedonia et al. [10]
93.0	3.335	This study
81.7	3.532	Smit [11]

Table 3

Gas–gas (1–1) and gas–solid (1–s) Lennard–Jones 12-6 potential parameters for small molecules interacting with oxygen atoms in siliceous materials

Gas	$T_c$ (K)	$V_c$ , (cm <sup>3</sup> mol <sup>-1</sup> )	$\epsilon_{11}/k$ (K)	$\sigma_{11}$ , (Å)	$\epsilon_{1s}/k$ ,	$\sigma_{1s}$ , (Å)
N <sub>2</sub>	126.2	89.5	100.2	3.613	85.1	3.439
CO	132.9	93.1	105.6	3.661	87.3	3.463
Ar	150.8	74.9	119.8	3.405	93.0	3.335
O <sub>2</sub>	154.6	73.4	122.8	3.382	94.2	3.324
CH <sub>4</sub>	190.6	99.0	151.4	3.737	104.5	3.501
Kr	209.4	91.2	166.4	3.636	109.6	3.450
CO <sub>2</sub>	304.2	94.0	241.7	3.673	132.1	3.469

the channels of silicalite. The Lennard–Jones potential parameters for the gas–solid interactions were calculated from Eqs. (10)–(13) based upon the reference value for argon–oxygen in Table 1. The assumption of spherical symmetry, which is strictly correct only for Kr, should hold for small nonpolar molecules (O<sub>2</sub>, CH<sub>4</sub>). For the molecules which contain dipole or quadrupole moments (CO, N<sub>2</sub>, CO<sub>2</sub>), the neglect of electrostatic energy is questionable even in silicalite.

## 7. Comparison of potential parameters with experiment

Henry constants ( $B/kT$ ) calculated from the potential parameters in Table 3 are compared with experiment in Table 4. For the nonpolar spherical molecules (O<sub>2</sub>, CH<sub>4</sub>, Kr) the average absolute error is 5%. The approximately spherical but polar molecules (CO, N<sub>2</sub>, CO<sub>2</sub>) exhibit an average error of about –10%. A similar trend is observed for the isosteric heats, whose values calculated from Table 3 are compared with experiment in Table 5. As in the case of the Henry constants, the predicted isosteric heats agree with experiment for the nonpolar spherical molecules (O<sub>2</sub>, CH<sub>4</sub>) but are about 10% too small for polar molecules (CO<sub>2</sub>, N<sub>2</sub>). Evidently the neglect of electrostatic energy of polar molecules in silicalite generates an error of about 10% in both the Henry constant and the energy of adsorption.

Simulated adsorption isotherms for methane on silicalite are shown in Fig. 3. The almost perfect agreement of the simulations with experimental

data from different laboratories using calculated (not fitted) potential parameters is encouraging. The quantitative agreement of simulations with experiment for nonpolar spherical molecules is attributed to: (1) extracting potential parameters from a well characterized reference system (argon on silicalite); and (2) converting simulation variables to experimental variables.

Simulated adsorption isotherms for krypton on silicalite are shown in Fig. 4. As in the case of methane, the agreement with experiment is almost perfect.

In summary, the Lennard–Jones potential parameters in Table 3 for small, spherical, nonpolar molecules (Ar, Kr, O<sub>2</sub>, CH<sub>4</sub>) agree quantitatively with experiments from different laboratories and are consistent with Lorentz–Berthelot mixing rules. The potential parameters determined for silicalite should in principle apply to other siliceous materials such as TON, MTW, UTD-1, FER, FAU, and MCM-41; the portability of the potential parameters will be investigated in a future paper.

## 8. Adsorption and density profiles in silicalite micropores

Dimensionless potential energies ( $\phi/kT$ ) are plotted for methane in silicalite at 32.6°C on Fig. 5. Points plotted parallel to the pore axes are the simulation-average total energy of adsorbate molecules located in each of 50 slices of space perpendicular to the pore axis. The total energy is the sum of gas–gas and gas–solid energies. The

Table 4

Comparison of Henry constants ( $B/kT$ ) from simulation with experimental data

Gas	$T$ (°C)	$B/kT$ (mol per (kg kpa))		Error (%)	References
		Experimental	Simulated		
$O_2$	32.3	0.00162	0.00170	5	(Dunne et al. [7])
$CH_4$	3.8	0.0176	0.0169	−4	(Sun et al. [13])
	23.1	0.00975	0.00957	−2	(Dunne et al. [7])
	31.0	0.00711	0.00773	9	(Golden and Sircar [9])
	69.9	0.00308	0.00313	2	(Golden and Sircar [9])
	79.6	0.00264	0.00254	−4	(Sun et al. [13])
$Kr$	32.3	0.00691	0.00783	13	(Golden and Sircar [9])
	69.4	0.00349	0.00332	−5	(Golden and Sircar [9])
$N_2$	23.0	0.00238	0.00196	−18	(Dunne et al. [7])
	31.9	0.00180	0.00164	−9	(Golden and Sircar [9])
	68.7	0.000947	0.000826	−13	(Golden and Sircar [9])
$CO$	32.3	0.00259	0.00206	−20	(Golden and Sircar [9])
	68.4	0.00129	0.00103	−21	(Golden and Sircar [9])
$CO_2$	3.8	0.111	0.0986	−11	(Sun et al. [13])
	31.4	0.0385	0.0381	−1	(Golden and Sircar [9])
	68.4	0.0137	0.0135	−2	(Golden and Sircar [9])
	79.6	0.0119	0.0101	−15	(Sun et al. [13])

planes dividing pore space into channels and intersections were determined by the saddle point of minimum potential energy trajectories along the axis of the main and side channels. The distance between the centers of the channel intersections is about 10 Å for both channels; only half of the main channel is plotted because of symmetry about its center at 0 Å. The center of the intersection at 5 Å for the main channel and at 0 and 10 Å for the side channel is the same point but the values of energy are slightly different because the main and side channels intersect at an angle and the space sampled perpendicular to the axis of the each channel is slightly different.

The decrease in potential energy with increasing pressure shown on Fig. 5 is due mainly to gas–gas interactions. The absolute value of the gas–gas interaction energy, which is zero at the limit of zero pressure, increases with pressure but is less

than  $kT$  even at high pressure. The variation in energy at constant pressure along the pore axes is about  $2kT$ . A diffuse minimum in energy, about  $2kT$  lower than the energy at the center of the channel intersection, occurs at the centers of the main and side channels. These positions within

Table 5

Comparison of isosteric heats from simulation with experimental data measured by calorimetry (Dunne et al. [7]) at 25°C and at limit of zero coverage

Gas	$Q_{st}$ (kJ mol <sup>−1</sup> )		Error (%)
	Experimental	Simulated	
$O_2$	16.3	15.5	−5
$CH_4$	20.9	20.1	−4
$CO_2$	27.2	24.3	−12
$N_2$	17.6	15.9	−11

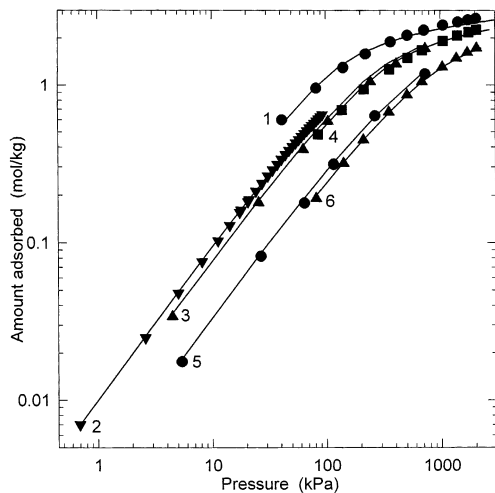


Fig. 3. Comparison of experimental points (Dunne et al. [7], Golden and Sircar [9], Sun et al. [13]) with simulations (solid lines) for adsorption of methane in silicalite. Simulation data converted to excess adsorption by Eq. (1). Line 1, 3.8°C; Line 2, 23.07°C; Line 3, 31.0°C; Line 4, 34.8°C; Line 5, 69.6°C; Line 6, 79.6°C.

the main and side channels are therefore energetically preferred ‘sites’ at low loading.

Fig. 6 shows the simulation average loading of

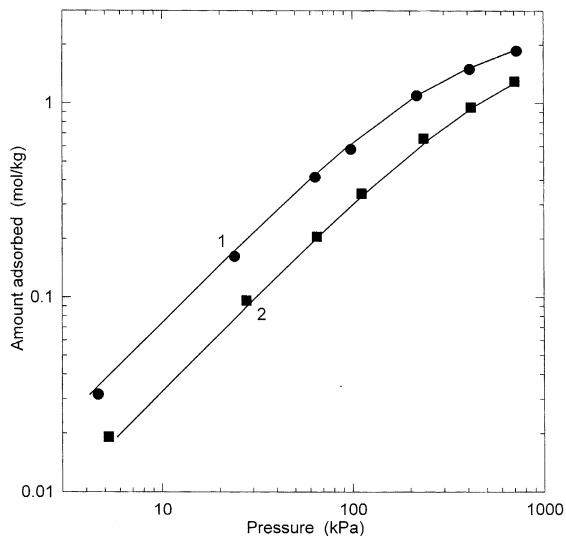


Fig. 4. Comparison of experimental points (Golden and Sircar [9]) with simulations (solid lines) for adsorption of Krypton on silicalite. Simulation data converted to excess adsorption by Eq. (1). Line 1, 32.3°C; Line 2, 69.4°C.

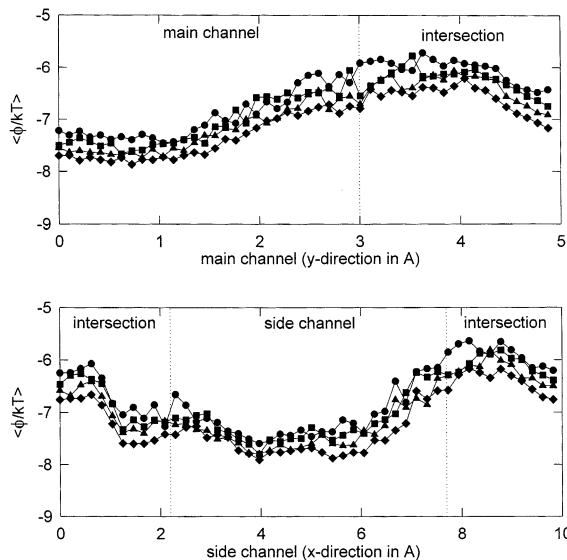


Fig. 5. Dimensionless simulation-averaged potential energy of methane in silicalite at 32.6°C as a function of distance along axes of straight main channel and zig-zag side channel. ●, 100 kPa; ■, 200 kPa; ▲, 400 kPa; ◆, 1000 kPa.

methane in silicalite. As expected, the local absolute amount adsorbed increases with pressure. (The experimental excess loadings are plotted on

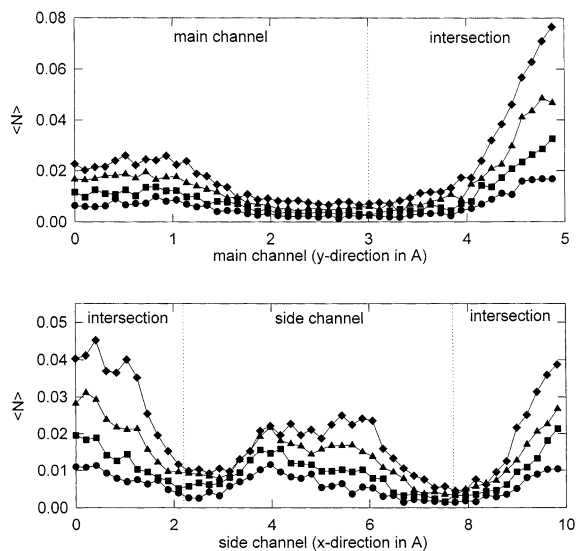


Fig. 6. Simulation-averaged amount of methane adsorbed in sections of main and side channels of silicalite at 32.6°C. Legend, same as Fig. 5.

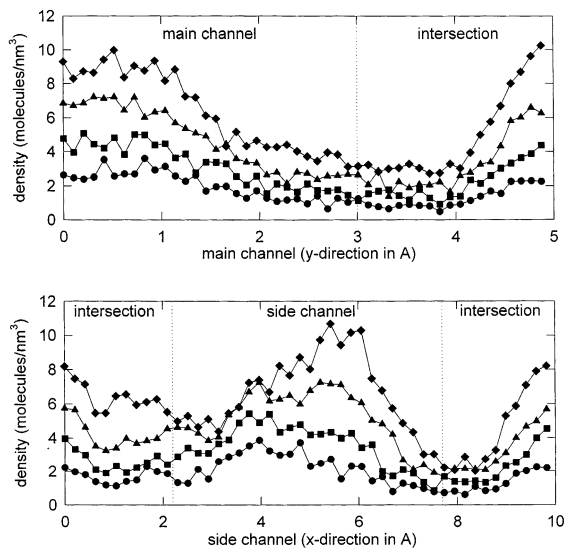


Fig. 7. Simulation-averaged local density of methane in main and side channels of silicalite at 32.6°C. Legend, same as Fig. 5.

Fig. 3). At constant pressure, the local amount adsorbed has a maximum near the center of each channel located at the minimum in the potential energy. However, the amount adsorbed is much higher within the intersection because it contains more space than the nearly one-dimensional channels. Even at low loading, the majority of the molecules adsorb in the intersections where the energy is higher (energetically less favorable) but more space is available.

Fig. 7 shows the ensemble-average density of methane in silicalite obtained by dividing the ensemble-average number of molecules in Fig. 6 by the volume of each space. The volume of each sample space was calculated from Eq. (2) by helium simulations similar to the determination of the total pore volume. The absolute density is highest near the center of each channel and at the center of the intersection where the potential energies have local minima. Conversion of the excess adsorption from Fig. 3 at 1000 kPa and 32.6°C using Eq. (1) gives an absolute adsorption of about  $2 \text{ mol kg}^{-1}$ . Based upon its pore volume of  $0.175 \text{ cm}^3 \text{ g}^{-1}$ , the average absolute pore density under these conditions is  $0.170 \text{ g cm}^{-3}$ . The maximum density from Fig. 7 (10 molecule per  $\text{nm}^3$ ) is

$0.266 \text{ g cm}^{-3}$ . These pore densities may be compared with the density of liquid methane at its normal boiling point, which is  $0.425 \text{ g cm}^{-3}$ . Thus, at 32.6°C and 1000 kPa, the average and maximum local absolute densities of methane in the pores are 40 and 62% of the liquid density, respectively. The pore density is high considering that the reduced temperature of methane is  $T/T_c = 305.75/190.4 = 1.60$ . Another interesting observation from Fig. 7 is the fivefold variation in local density.

Fig. 8 shows a comparison of ensemble-average densities for He, Ar, Kr, and  $\text{CH}_4$  at 32.6°C. The average absolute loading at the indicated pressures is about  $2 \text{ mol kg}^{-1}$  for methane and krypton so their profiles nearly coincide. The average absolute loading for argon at 800 kPa is about one-half the value for methane and krypton. The absolute pore density of helium is equal to the density of gaseous helium at 500 kPa and 32.6°C:  $0.118 \text{ molecules per nm}^3$ . Therefore, (within 1% of the total) no helium is adsorbed under these conditions; the excess adsorption of helium is zero (Talu and Myers [4]).

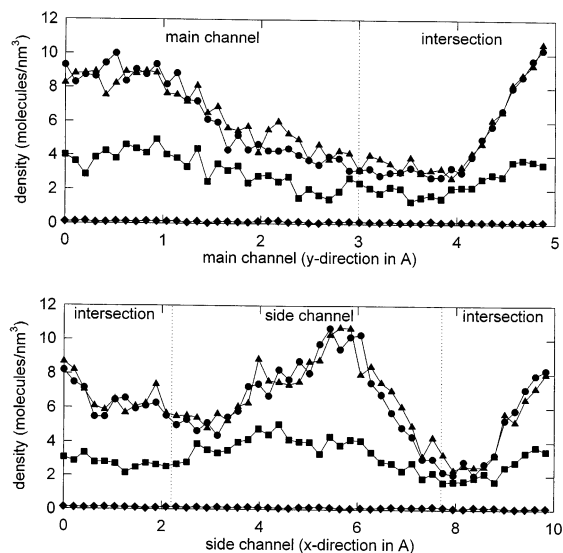


Fig. 8. Simulation-averaged local density of helium, argon, krypton, and methane in main and side channels of silicalite at 32.6°C. ●,  $\text{CH}_4$  at 1000 kPa; ▲, Kr at 800 kPa; ■, Ar at 800 kPa; ◆, He at 500 kPa.

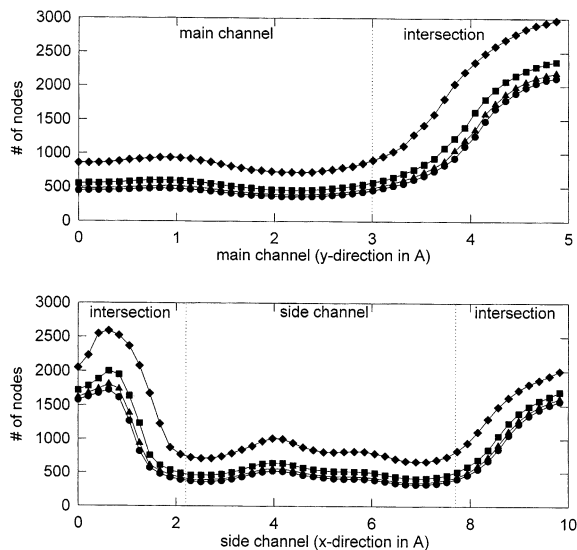


Fig. 9. Volume available for adsorption ( $\phi < 0$ ) in 50 sections of main and side channels of silicalite measured by helium, argon, krypton, and methane molecules. Legend, same as Fig. 8.

Fig. 9 shows the profile of the pore volume in each of the 50 spaces perpendicular to the axes of the channels as determined by four molecules: helium, argon, krypton, and methane. The local pore size was defined as the number of nodes with potential energy less than zero, counted from a pre-tabulation of dispersion energies on a 3-dimensional grid with a spacing of 0.01 Å. As expected, the accessible pore volume decreases with the size of the molecule. Fig. 9 emphasizes the necessity for selecting a non-adsorbing reference molecule. Having selected a reference molecule (helium) and having found conditions under which its excess adsorption is negligible ( $T > 300$  K and  $P < 1$  bar), simulations can be compared with experiment without ambiguity.

## 9. Conclusions

- The Lennard–Jones 12-6 potential parameters for argon–oxygen interactions in siliceous materials like silicalite are  $\epsilon/k = 93.0$  K and  $\sigma = 3.335$  Å. Parameters for other small nonpolar

molecules (He, O<sub>2</sub>, Kr, CH<sub>4</sub>) are derived from Lorentz–Berthelot mixing rules using the principle of corresponding states. These potential constants for small nonpolar molecules are in quantitative agreement with experiment for silicalite and in principle should predict adsorption of small nonpolar molecules in other siliceous materials (TON, MTW, UTD-1, FER, FAU, MCM-41).

- The absolute local density of supercritical gases (Ar, Kr, CH<sub>4</sub>) adsorbed in silicalite at high loading and room temperature is about half the density of the liquids at their normal boiling points.
- The quantitative agreement of the reference potentials with experiment for nonpolar spherical molecules is attributed to the conversion of absolute simulation variables to excess experimental variables for the well-characterized reference system of argon on silicalite.
- The pore volume of silicalite from the helium–oxygen potential is 0.175 cm<sup>3</sup> g<sup>-1</sup>.

## Acknowledgements

Financial support was provided by National Science Foundation Grant NSF CTS-0080915 (Myers) and CTS-9725256 (Talu).

## References

- [1] A.L. Myers, J. Calles, G. Calleja, Comparison of molecular simulation of adsorption with experiment, *Adsorption* 3 (1997) 107–115.
- [2] S. Sircar, Excess properties and thermodynamics of multi-component gas adsorption, *J. Chem. Soc. Faraday Trans.* 181 (1985) 1527–1540.
- [3] S. Sircar, Revisiting Gibbs excess for adsorption, *Ind. Eng. Chem. Res.* 38 (1999) 3670–3682.
- [4] O. Talu, A.L. Myers, Molecular simulation of adsorption: Gibbs dividing surface and comparison with experiment, *AIChE J.*, (2000) in press.
- [5] A.V. Neimark, P.I. Ravikovitch, Calibration of pore volume in adsorption experiments and theoretical models, *Langmuir* 13 (1997) 5148–5160.
- [6] D.H. Olson, G.T. Kokotailo, S.L. Lawton, W.M. Meier, Crystal structure and structure related properties of ZSM-5, *J. Phys. Chem.* 85 (1981) 2238–2243.

- [7] J.A. Dunne, R. Mariwala, M. Rao, S. Sircar, R.J. Gorte, A.L. Myers, Calorimetric heats of adsorption and adsorption isotherms. I. O<sub>2</sub>, N<sub>2</sub>, Ar, CO<sub>2</sub>, CH<sub>4</sub>, C<sub>2</sub>H<sub>6</sub>, and SF<sub>6</sub> on silicalite, *Langmuir* 12 (1996) 5888–5895.
- [8] J.O. Hirschfelder, C.F. Curtiss, R.B. Bird, *Molecular Theory of Gases and Liquids*, Wiley, New York, 1954, p. 1114.
- [9] T.C. Golden, S. Sircar, Gas Adsorption in Silicalite, *J. Coll. Interf. Sci.* 162, (1994) 182–188.
- [10] M.D. Macedonia, D.D Moore, E.J. Maginn, Adsorption studies of methane, ethane, and argon in the zeolite mordenite: molecular simulations and experiments, *Langmuir* 16 (2000) 3823–3834.
- [11] B. Smit, Simulating the adsorption isotherms of methane, ethane, and propane in the zeolite silicalite, *J. Phys. Chem.* 99 (1995) 5597–5603.
- [12] R.C. Reid, J.M. Prausnitz, B.E. Poling, *The Properties of Gases and Liquids*, Fourth Ed., McGraw-Hill, New York, 1987, p. 656.
- [13] M.S. Sun, D.B. Shah, H.H. Xu, O. Talu, Adsorption equilibria of C1 to C4 alkanes, CO<sub>2</sub>, and SF<sub>6</sub> on silicalite, *J. Phys. Chem. B* 102 (1998) 1466–1473.